Chemical Science

PERSPECTIVE

Check for updates

Redox catalysis *via* photoinduced electron transfer

Yong-Min Lee, [*ab] Wonwoo Nam [*a] and Shunichi Fukuzumi [*a]

This perspective article highlights redox catalysis of organic and inorganic molecules *via* photoinduced electron transfer, which is well exploited for a number of important photoredox reactions including hydrogen evolution, water oxidation and a number of synthetic applications. Organic and inorganic photoredox catalysis is also combined with thermal transition metal redox catalysis to achieve overall photocatalytic redox reactions, which would otherwise not be possible by using photoredox catalysis or thermal redox catalysis alone. Both thermodynamic and kinetic data are discussed to understand the photoinduced electron-transfer processes of organic and inorganic photoredox catalysts in the light of the Marcus theory of electron transfer, providing a comprehensive and valuable guide for employing organic and inorganic redox catalysts *via* photoinduced electron transfer. The excited states of electron donors including radicals and anions act as super-reductants in the photoinduced electron-transfer reactions, whereas the excited states of electron acceptors including cations act as super-oxidants in the photoinduced electron-transfer reactions. Photoexcitation of simple electron donor–acceptor linked molecules with small reorganization energies of electron transfer results in formation of long-lived electron-transfer states, which can oxidize and reduce substrates to make various chemical transformations possible with use of transition metal redox catalysis. Finally molecular model systems of photosystems I and II are combined to achieve water splitting to evolve H_2 and O_2.

1 Introduction

Solar energy conversion in photosynthesis has been achieved by photoinduced multi-step charge-separation processes in the photosynthetic reaction centers (PRCs) in Photosystem II (PS-II), where electrons and protons are taken from water.[1–4] These electrons and protons are used to generate a proton gradient and reduce $NADP^+$ to NADPH *via* redox shuttle reactions in Photosystem I (PS-I) through the Z scheme, leading to the reduction of CO_2 into carbohydrates.[1,4] There

aDepartment of Chemistry and Nanoscience, Ewha Womans University, Seoul, 03760, Korea. E-mail: yomlee@ewha.ac.kr; wwnam@ewha.ac.kr; fukuzumi@chem.eng.osaka-u.ac.jp

bResearch Institute for Basic Sciences, Ewha Womans University, Seoul, 03760, Korea

Yong-Min Lee obtained his PhD in inorganic chemistry from Pusan National University in 1999 under the guidance of Professor Sung-Nak Choi. In 1999, he moved to the Center for Magnetic Resonance (CERM) at the University of Florence (Italy) as Postdoctoral fellow and Researcher under the supervision of Professor Claudio Luchinat and Professor Ivano Bertini. In 2006, he joined the Center for Dioxygen Chemistry at Ewha Womans University. Since 2009, he has been working at Ewha Womans University as a Special Appointment Professor. His research has been focusing on the roles of metal ions in biological systems.

Wonwoo Nam earned his PhD degree in Inorganic Chemistry from the University of California, Los Angeles (UCLA) under the supervision of Professor Joan S. Valentine in 1990. After working for one year as a postdoctoral fellow at UCLA, he was appointed an Assistant Professor at Hong Ik University in 1991. In 1994, he moved to Ewha Womans University, where he is currently a Distinguished Professor. His current research has been focusing on dioxygen activation, water oxidation, and important roles of metal ions in bioinorganic chemistry.

have been extensive studies to mimic the charge-separation processes in PRCs using covalently and non-covalently linked organic electron donor–acceptor molecules.[5–17] Photoexcitation of donor–acceptor linked molecules (D–A) results in electron transfer from the excited state of electron donor (D*) or acceptor (A*) to an electron acceptor (A) or donor (D) to produce the charge-separated state (D$^{\bullet+}$–A$^{\bullet-}$), which has both oxidizing ability due to D$^{\bullet+}$ and the reducing ability due to A$^{\bullet-}$.[4] Photoexcitation of metal complexes composed of an electron donor metal (M^{n+}) and electron acceptor ligand (L) also results in generation of the metal-to-ligand charge-transfer (MLCT) state (M$^{(n+1)+}$L$^{\bullet-}$), which has both oxidizing ability due to M$^{(n+1)+}$ and the reducing ability due to L$^{\bullet-}$.[18–20] In the presence of an electron donor substrate (S$_D$) and an electron acceptor substrate (S$_A$), electron transfer from S$_D$ to D$^{\bullet+}$–A$^{\bullet-}$, produced by photoexcitation of D–A [eqn (1)], results in formation of S$_D^{\bullet+}$ and D–A$^{\bullet-}$ [eqn (2)], which transfers an electron to S$_A$ to produce S$_A^{\bullet-}$, accompanied by regeneration of D–A [eqn (3)].[21–23] A bond formation between S$_D^{\bullet+}$ and S$_A^{\bullet-}$ may occur [eqn (4)] in competition with back electron transfer from S$_A^{\bullet-}$ to S$_D^{\bullet+}$ [eqn (5)].[21–23] In such a case, the overall reaction is the photocatalytic bond formation reaction between S$_D$ and S$_A$ with D–A, which acts as an organic photoredox catalyst [eqn (6)].[21–23] D–A can be replaced by a metal complex (M^{n}L) that affords the MLCT excited state upon photoexcitation.[18–20]

$$D-A \xrightarrow{h\nu} D^{\bullet+}-A^{\bullet-} \tag{1}$$

$$S_D + D^{\bullet+}-A^{\bullet-} \rightarrow S_D^{\bullet+} + D-A^{\bullet-} \tag{2}$$

$$S_A + D-A^{\bullet-} \rightarrow S_A^{\bullet-} + D-A \tag{3}$$

$$S_D^{\bullet+} + S_A^{\bullet-} \rightarrow S_D-S_A \tag{4}$$

$$S_D^{\bullet+} + S_A^{\bullet-} \rightarrow S_D + S_A \tag{5}$$

$$S_D + S_A \xrightarrow[D-A]{h\nu} S_D-S_A \tag{6}$$
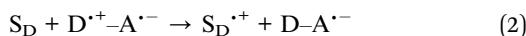
Shunichi Fukuzumi received his bachelor's degree and PhD degree at Tokyo Institute of Technology in 1973 and 1978, respectively. After working as a postdoc at Indiana University in the USA (1978–1981), he became an Assistant Professor at Osaka University. He was promoted to a Full Professor in 1994 and a Distinguished Professor in 2013. His research has been focusing on artificial photosynthesis. He is currently a Professor of Ewha Womans University and a Professor Emeritus of Osaka University.

A substrate radical cation (S$_D$H$^{\bullet+}$), which is produced by electron transfer from S$_D$H to D$^{\bullet+}$–A$^{\bullet-}$ [eqn (7)], can react with a nucleophile (NH) to produce the adduct radical (S$_D$–NH$^{\bullet}$) and H$^+$ [eqn (8)].[21] On the other hand, S$_A^{\bullet-}$, which is produced by electron transfer from D–A$^{\bullet-}$ to S$_A$ [eqn (3)], is protonated to produce S$_A$H$^{\bullet}$ [eqn (9)].[21] Then, hydrogen atom transfer from S$_D$–NH to S$_A$H$^{\bullet}$ yields S$_D$–N and S$_A$H$_2$ [eqn (10)].[21] The overall reaction is the photocatalytic bond formation between S$_D$H and NH with D–A, accompanied by the reduction of S$_A$ to S$_A$H$_2$ [eqn (11)].[21] In this case as well, D–A can be replaced by M^{n}L.[21]

$$S_DH + D^{\bullet+}-A^{\bullet-} \rightarrow S_DH^{\bullet+} + D-A^{\bullet-} \tag{7}$$

$$S_DH^{\bullet+} + NH \rightarrow S_D-NH^{\bullet} + H^+ \tag{8}$$

$$S_A^{\bullet-} + H^+ \rightarrow S_AH^{\bullet} \tag{9}$$

$$S_D-NH^{\bullet} + S_AH^{\bullet} \rightarrow S_D-N + S_AH_2 \tag{10}$$

$$S_DH + NH + S_A \xrightarrow[D-A]{h\nu} S_D-N + S_AH_2 \tag{11}$$
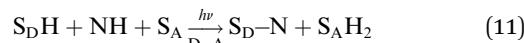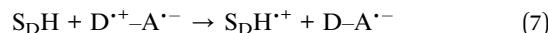
Both the photocatalytic bond formation between S$_D$ and S$_A$ [eqn (6)] and that between S$_D$H and NH, accompanied by the reduction of S$_A$ to S$_A$H$_2$ [eqn (3), (9) and (10)] are started by electron transfer from substrates (S$_D$ and S$_D$H) to D$^{\bullet+}$–A$^{\bullet-}$ (or M$^{(n+1)+}$L$^{\bullet-}$) to produce S$_D^{\bullet+}$ and S$_D$H$^{\bullet+}$ [eqn (2) and (7)], respectively.[19] Electron transfer from D–A$^{\bullet-}$ to S$_A$ should also occur to regenerate D–A [eqn (3)].[21] Although there have been many studies on the photocatalytic reactions with D–A and M^{n}L, the thermodynamics and kinetics of electron transfer between substrates and D$^{\bullet+}$–A$^{\bullet-}$ (or M$^{(n+1)+}$L$^{\bullet-}$) have yet to be summarized by a systematic manner. In this review, we focus on the thermodynamics and kinetics of electron transfer between substrates (S$_D$ and S$_D$H) and D$^{\bullet+}$–A$^{\bullet-}$ (or M$^{(n+1)+}$L$^{\bullet-}$) [eqn (2), (3) and (7)], providing quantitative basis to predict the photocatalytic bond formation reactions [eqn (4) and (8)].

In the photocatalytic reactions, D–A acts as a photoredox catalyst [eqn (2) and (3)]. In these cases, D and A are not necessarily linked together. Photoinduced electron transfer from D to the excited state of A (A*) or photoinduced electron transfer from the excited state of D (D*) to A occurs to produce D$^{\bullet+}$ and A$^{\bullet-}$, which enable photocatalytic bond formation reactions [eqn (4) and (8)]. Once reactive species such as D$^{\bullet+}$ and A$^{\bullet-}$ are produced, various redox reactions are made possible to occur *via* D$^{\bullet+}$ and A$^{\bullet-}$. This perspective focuses on photoinduced electron transfer reactions of D, A and D–A, which initiate various photoredox catalytic reactions. The rate constants of photoinduced electron transfer and back electron transfer are evaluated in light of the Marcus theory of electron transfer.[24–26] Firstly electron transfer from D*, which are super-reductants, to A is discussed with the photoredox catalytic mechanisms. Secondly electron transfer from D to A*, which are super-oxidants, is discussed with the photoredox catalytic mechanisms. Finally photoredox catalytic reactions with PRC models (D–A) are discussed to show the combination of PS-I and PS-II models.

2 Super-reductants

2.1. Singlet excited states of NADH analogs

The singlet excited state of an NADH (dihydronicotinamide adenine dinucleotide) analog, 9,10-dihydro-10-methylacridine (^{1}AcrH$_2^*$), has a largely negative one-electron reduction potential (-3.1 V $vs.$ SCE) and an appreciable lifetime of 7.0 ns.[27] Electron transfer from ^{1}AcrH$_2^*$ to various halogenated compounds (RX) occurs to produce dehalogenated compounds (RH) and the two-electron oxidation product, 10-methyl-acridinium ion (AcrH$^+$), because the one-electron reduction potentials of RX are less negative ($e.g.$, -2.78 V $vs.$ SCE) than that of ^{1}AcrH$_2^*$ (-3.1 V $vs.$ SCE).[27] The rate constant of electron transfer from ^{1}AcrD$_2^*$ to PhCl was determined to be 6.0×10^8 M^{-1} s^{-1} at 298 K from the fluorescence quenching by PhCl.[27] When AcrH$_2$ was replaced by the dideuterated compound (AcrD$_2$), the rate constant of electron transfer from ^{1}AcrD$_2^*$ to PhCl was the same as that of ^{1}AcrH$_2^*$, showing no deuterium kinetic isotope effect.[27] Electron transfer reduction of RX results in the C–X bond cleavage to produce R$^•$ and X$^-$.[28] The produced carbon-centered radical (R$^•$) abstracts a hydrogen atom from AcrH$_2^{•+}$, which is produced by electron transfer from ^{1}AcrH$_2^*$ to RX, to form 10-methylacridinium ion (AcrH$^+$) and RH [eqn (12)].[27]

$$\text{(structure)} + RX \xrightarrow{h\nu} \text{(structure)} + X^- + RH \qquad (12)$$
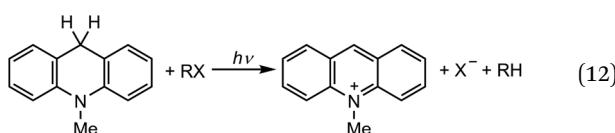
Because AcrH$^+$ can be reduced by NaBH$_4$ to regenerate AcrH$_2$ [eqn (13)], AcrH$_2$ acts as an organic photoredox catalyst for photocatalytic dehalogenation of RX by NaBH$_4$.[27]

$$NaBH_4 + AcrH^+ \rightarrow AcrH_2 + Na^+ + BH_3 \qquad (13)$$
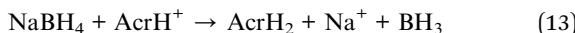
Photoredox catalysis of AcrH$_2$ was applied to trifluoromethylation of hydrazones with an electrophilic CF$_3$-transfer reagent (CF$_3$SO$_2$Cl) as shown in Scheme 1.[29] Upon photoexcitation of AcrH$_2$ in the presence of CF$_3$SO$_2$Cl, electron transfer from ^{1}AcrH$_2^*$ (E_{ox}^* $vs.$ SCE $= -3.1$ V) to CF$_3$SO$_2$Cl (E_{red} $vs.$ SCE $= -0.18$ V) occurs rapidly to produce AcrH$_2^{•+}$, CF$_3^•$ and SO$_2$Cl$^-$, followed by radical addition of CF$_3^•$ to the C=N bond to produce aminyl radical intermediate B in Scheme 1, which is stabilized by the lone pair of the adjacent nitrogen atom. B is oxidized by AcrH$_2^{•+}$ to afford nitrenium intermediate C in Scheme 1, accompanied by regeneration of AcrH$_2$. Finally, intermediate C undergoes deprotonation with a base to yield the trifluoromethylated product (Scheme 1).[29]

The photoredox catalysis of AcrH$_2$ was combined with palladium catalysis for arylation of arenes with aryldiazonium salts (Scheme 2).[30] Photoirradiation of a methanol solution containing AcrH$_2$, ArN$_2$BF$_4$, and Pd(OAc)$_2$ with blue LED light for 12 h afforded C–H arylation product (86% yield).[30] The reaction was initiated by electron transfer from ^{1}AcrH$_2^*$ to ArN$_2$BF$_4$ to generate AcrH$_2^{•+}$ and Ar$^•$, accompanied by N$_2$
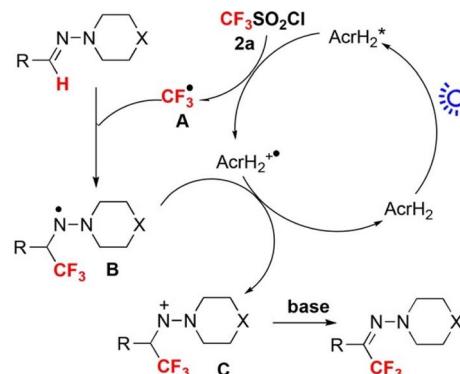
Scheme 1 Photocatalytic trifluoromethylation of hydrazones with an electrophilic CF$_3$–transfer reagent (CF$_3$SO$_2$Cl) by AcrH$_2$ photoredox catalysis. Reprinted from ref. 29 with permission form John Wiley and Sons (Copyright 2017).
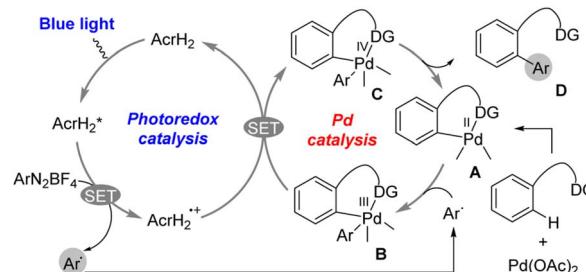
Scheme 2 Photocatalytic arylation of C–H bond by incorporating a palladium catalyst and AcrH$_2$ photoredox catalyst. Reprinted from ref. 30 with permission form American Chemical Society (Copyright 2017).

dissociation (Scheme 2).[30] Ar$^•$ reacts with complex A in Scheme 2 to afford the palladium(III) complex B, which is then oxidized by AcrH$_2^{•+}$ via electron transfer from complex B to AcrH$_2^{•+}$ to produce palladium(IV) complex C and regenerate the photocatalyst AcrH$_2$ (Scheme 2).[30] Finally, the reductive elimination of palladium(IV) complex C affords the formation of compound D, which is the arylated product, and regenerates the palladium(II) catalyst A.[30] Thus, a dual catalytic system of palladium(II)/organic photoredox catalysts enables the arylation of arenes with ArN$_2^+$ over a wide substrate range under the mild conditions.[30]

The singlet excited state of 1-benzyl-1,4-dihydronicotinamide (BNAH), which is one of the NADH analogs, can also be used as a strong one-electron reductant for the photoinduced reduction of substrates, although the one-electron oxidation potential (-2.6 V $vs.$ SCE)[31] is less negative than that of ^{1}AcrH$_2^*$ (-3.1 V $vs.$ SCE).[27] BNAH or BNA$^+$ is used as a photoredox catalyst for hydrogenation of α,β-epoxy ketones and 1,2-diketones with HCO$_2$H and Et$_3$N to produce β-hydroxy and α-hydroxy ketones,[32] because BNA$^+$ can be converted to BNAH by a mixture of HCO$_2$H/Et$_3$N at room temperatures.[33] The photocatalytic hydrogenation mechanism by BNAH is shown in Scheme 3. Firstly, electron transfer from ^{1}BNAH* to α,β-epoxy ketone (compound **1** in Scheme 3) or benzil ($i.e.$,
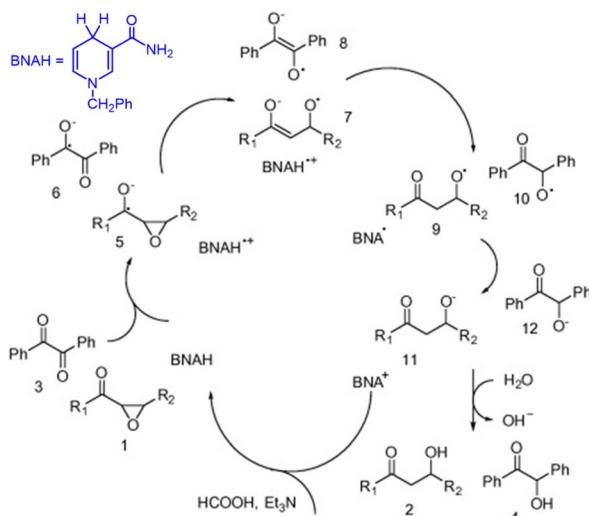
Scheme 3 Photocatalytic hydrogenation of α,β-epoxy ketones to β-hydroxy ketones with HCO_2H and Et_3N by BNAH photoredox catalysis. Reproduced from ref. 33 with permission form American Chemical Society (Copyright 2006).

diphenylethanedione; compound **3** in Scheme 3) occurs to produce BNAH[•+] and the radical anions of compounds **1** and **3** (species **5** and **6** in Scheme 3, respectively). Then, the carbon–oxygen bond cleavage occurs to convert species **5** (or species **6**) into species **7** (or species **8**), followed by proton transfer from BNAH[•+] to species **7** (or species **8**) and an enol/keto tautomerization to produce species **9** (or species **10**) and BNA[•] (Scheme 3). Because BNA[•] is a strong one-electron reductant,[34] electron transfer from BNA[•] to species **9** (or species **10**) to produce species **11** (or species **12**), accompanied by regeneration of BNA[+].[33] The protonation of species **11** (or species **12**) by water yields the final products (compounds **2** and **4** in Scheme 3).[33]

2.2. Doublet excited states of radicals

10-Methylacridinyl radical acts as a relatively strong reductant (E_{red} vs. SCE = −0.43 V),[35] being unstable due to the fast dimerization reaction. However, 9-phenyl-10-methylacridinyl radical is stable due to the steric effect of 9-Ph moiety that prohibits the dimerization reaction.[36] 3,6-Di-^{t}Bu-9-mesityl-10-phenylacridinium tetra-fluoroborate, [Mes-(10-Ph)Acr](BF_4), also provides the stable acridinyl radical (Mes-(10-Ph)Acr[•]) upon the one-electron reduction of [Mes-(10-Ph)Acr](BF_4).[37] If the doublet excited state of the stable acridinyl radical ([Mes-(10-Ph)Acr[•]]*) can be used as a reductant, the most negative E_{red} value was estimated to be −3.36 V vs. SCE.[37] Such an extremely strong one-electron reductant has enabled to develop reductive dehalogenation of aryl halides even with electron-donating substituents to afford the desired dehalogenated products in good to excellent yields.[37] As shown in Scheme 4, upon photoexcitation of [Mes-(10-Ph)Acr](BF_4), electron transfer from diisopropylamine (^{i}Pr$_2$NEt) to the Acr[+] moiety of the electron-transfer state of [Mes-(10-Ph)Acr](BF_4) occurs to produce ^{i}Pr$_2$NEt[•+] and the stable acridinyl radical (Mes-(10-Ph)Acr[•]).[37] The acridly radical
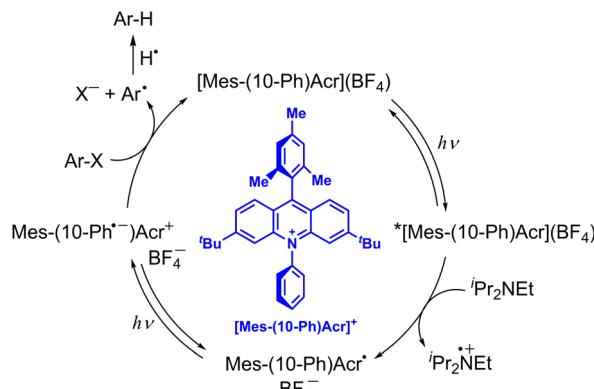
Scheme 4 Reductive dehydrogenation of aryl halide (Ar–X) with diisopropylamine by photoredox catalysis of [Mes-(10-Ph)Acr](BF_4).[37]

is photoexcited to produce the charge-separated state in which the phenyl moiety becomes the phenyl radical anion (Mes-(10-Ph[•−])Acr[+]) that is capable to undergo dissociative electron transfer to Ar–X to produce aryl radical (Ar[•]) and X[−].[37] Aryl radical abstracts hydrogen atom from ^{i}Pr$_2$NEt[•+] to produce Ar–H and regenerate the photocatalyst {[Mes-(10-Ph)Acr](BF_4)}.[37] When p-methoxychlorobenzene, which exhibits a largely negative half-peak potential (<−2.8 V vs. SCE), is employed as a substrate, the yield of p-methoxybenzene was 82%.[37] This indicates that electron transfer from the excited state of the acridinyl radical ([Mes-(10-Ph)Acr[•]]*) to p-methoxychlorobenzene may occur efficiently.[37] However, the lifetime of [Mes-(10-Ph)Acr[•]]* was much shorter than 100 ps. Fast electron transfer from the short-lived [Mes-(10-Ph)Acr[•]]* to p-methoxychlorobenzene has yet to be confirmed by femtosecond laser transient absorption spectroscopy. The reductive detosylation of amines was also made possible by using the doublet excited state of Mes-(10-Ph)Acr[•].[37]

The doublet excited state of perylene diimide radical anion (PDI[•−]) has also been used as a super-reductant that is capable of reducing aryl chlorides.[38] The strong reducing excited state (*PDI[•−]) was produced in situ by two subsequent visible light excitations starting from air-stable PDI, enabling to avoid the use of donor molecules, which are highly moisture- and air-sensitive. Only mixing of aryl chlorides (Ar–Cl compounds) with electron-withdrawing substituents, PDI and triethylamine (Et_3N) under irradiation with visible light afforded the reduced products (i.e., Ar–H products) with good to excellent yields.[38] The photocatalytic mechanism is shown in Scheme 5, where photoexcitation of a DMF solution containing PDI and Et_3N under 455 nm blue light results in electron transfer from Et_3N to PDI* to produce PDI[•−] that is stable in the absence of dioxygen.[38] PDI[•−] is excited again by visible light to produce *PDI[•−] and the dissociative electron transfer from *PDI[•−] to aryl halides undergoes, resulting that aryl chlorides are reduced to aryl radical (Ar[•]) species, which abstract a H-atom from Et_3N[•+] to yield Ar–H products.[38]

Transient absorption spectra of *PDI[•−] were observed upon excitation (λ_{ex} = 700 nm), exhibiting absorption bands at 460 and 600 nm due to ^{2}(PDI[•−])*.[39] The negative absorptions at 655–
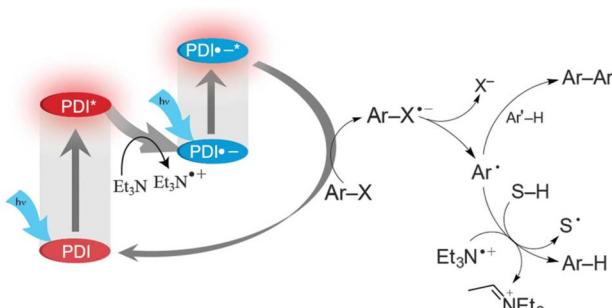
Scheme 5 Photocatalytic dehydrogenation of aryl halide (Ar–X) with triethylamine (Et$_3$N) by consecutive photoinduced electron-transfer processes with perylene diimides (PDIs). Reprinted from ref. 38 with permission form the American Association for the Advancement of Science (Copyright 2014).

Scheme 6 Reductive electrophotocatalysis with the photoexcited state of DCA$^{•-}$ (*DCA$^{•-}$) for the reductive borylation of aryl chlorides and aryl bromides with bis(pinacolato)diboron (B$_2$pin$_3$). Reprinted from ref. 42 with permission form American Chemical Society (Copyright 2010).

750 nm correspond to the ground state bleaching of PDI$^{•-}$.[39] The excited state absorption at 460 nm due to *PDI$^{•-}$ decayed, following first-order kinetics to give a lifetime (τ) of 160 ± 2 ps.[39] The lifetime decreased with increasing concentrations of electron acceptors (Fig. 1a).[39]

The dependence of logarithm of the quenching constants (k_q) of *PDI$^{•-}$ by electron transfer to electron acceptors on the 1 e$^-$ reduction potentials of electron acceptors [E°(A/A$^{•-}$)] is shown in Fig. 1b, where the k_q values of electron acceptors,

Fig. 1 (a) Stern–Volmer plots for lifetime quenching of *PDI$^{•-}$ versus concentrations of electron acceptors. (b) Dependence of logarithm of k_q of electron transfer from *PDI$^{•-}$ to electron acceptors on the 1 e$^-$ reduction potentials (E_{red} vs. SCE) of electron acceptors. Red line represents the fit calculated using the Rehm–Weller equation. Reprinted from ref. 39 with permission form American Chemical Society (Copyright 2020).

which have E°(A/A$^{•-}$) values of more than −1.5 V vs. SCE, approached the diffusion limited value (∼2 × 10^{10} M^{-1} s^{-1}).[39] On the other hand, the k_q values of electron acceptors, which have E°(A/A$^{•-}$) values of less than −1.5 V vs. SCE, exhibited the sharp drop in the region where E°(PDI/*PDI$^{•-}$) = E°(A/A$^{•-}$) (i.e., $\Delta G_{ET} = 0$).[39] The dependence of log k_q on E°(A/A$^{•-}$) was well fitted with E°(PDI/*PDI$^{•-}$) value of −1.87 V vs. SCE and λ value of 0.84 eV using the Rehm and Weller empirical equation, which was reexamined by Farid, Dinnocenzo, Merkel, Young, Shukla and Guirado,[40] that correlates k_q and ΔG_{ET} with the reorganization energy for electron transfer [$\lambda = 4 \times \Delta G^{\ddagger}(0)$] (red line in Fig. 1b).[39–41] Thus, *PDI$^{•-}$ is a strong one-electron reductant that can reduce electron acceptors, which have the E_{red} values of more than −1.7 V. However, electron transfer from *PDI$^{•-}$ to Ar–Cl was too slow to compete with the fast decay rate of ^{2}(PDI$^{•-}$)*.[39]

The photoexcited state of 9,10-dicyanoanthracene radical anion (*DCA$^{•-}$) is also estimated to have an exceptionally negative E^{*}_{red} value of −3.2 V vs. SCE, which is comparable to some of the most oxidizable elemental metals such as Li (E vs. SCE = −3.3 V).[42] In addition, *DCA$^{•-}$ has a lifetime (τ) of 13.5 ns, which is long enough to undergo electron transfer reduction of a wide range of Ar–X compounds with E_{red} values as low as −2.94 V vs. SCE (Scheme 6).[42] DCA$^{•-}$ was produced using an H-type split cell with a porous carbon cathode and a Zn plate sacrificial anode by applying a constant cell voltage of 3.2 V.[42] Photoirradiation of DCA$^{•-}$ in the cathodic compartment with use of blue light enabled efficient coupling of 4-chlorobenzoate and B$_2$pin$_3$ (pin = pinacolato) as a radical acceptor to yield arylboronate (88%).[42] This method has also been applied to the reductive borylation of 4-Cl-anisole, which has a very negative E_{red} value of −2.90 V vs. SCE.[42] The mesolytic cleavage of a C–Br bond is significantly faster than that of a C–Cl bond, so that 1-Br-4-Cl-benzene was selectively converted to boronated–debrominated product.[42]

2.3. Singlet excited states of organic anions

The electron-transfer reduction of naphthalene monoimide (NMI) gives the radical anion (NMI$^{•-}$), which has E_{ox} value of

Fig. 2 (a) Chemical scheme of the formation of a singlet excited state ([^{1}NMI(H)$^-$]*) from naphthalene monoimide (NMI) *via* a doublet excited state ([^{2}NMI$^{•-}$]*). (b) Energy level diagrams of NMI, [^{2}NMI$^{•-}$]* and [^{1}NMI(H)$^-$]* with redox potentials *vs.* Fc/Fc$^+$. Reprinted from ref. 43 with permission form American Chemical Society (Copyright 2021).

−1.7 V *vs.* Fc/Fc$^+$, in propylene carbonate (Fig. 2a).[43] The femtosecond laser induced transient absorption measurements revealed that the doublet excited state of the radical anion ([^{2}NMI$^{•-}$]*) has a lifetime (τ) of 24 ps, which was too short to undergo intermolecular photoredox reactions with substrates (Fig. 2a).[43] In contrast, the singlet excited state of the two-electron reduced anion ([^{1}NMI(H)$^-$]*) species, which is called Meisenheimer complex, has the fluorescence lifetime of 20 ns.[43] Together with a high excited state energy (−3.08 V *vs.* Fc/Fc$^+$ in Fig. 2b), such a long fluorescent lifetime has enabled [^{1}NMI(H)$^-$]* to act as a super-reductant that can reduce Ar–X compounds to afford the products of C–C and C–P bond coupling *via* photoinduced electron transfer.[43]

3 Super-oxidants

3.1. Excited states of quinones

The one-electron reduction potential of the triplet excited state (E^*_{red}) of 2,3-di-Cl-5,6-di-CN-*p*-benzoquinone (^{3}DDQ*) is 3.18 V *vs.* SCE, which is highly positive enough to oxidize benzene by electron transfer to produce benzene radical cation, which can react with nucleophiles such as OH$^-$ to yield phenol (Scheme 7).[44] Although electron transfer from benzene (E_{ox} *vs.*

SCE = 2.48 V) to DDQ at the ground state (E_{red} *vs.* SCE = 0.51 V) is highly endergonic, electron transfer from benzene to ^{3}DDQ* becomes exergonic to proceed.[44] Thus, photoirradiation of benzene together with DDQ and H$_2$O resulted in formation of phenol and DDQH$_2$ [eqn (14)].[44] ^{t}Butyl nitrite (TBN) was used as a recycling reagent to oxidize DDQH$_2$ to regenerate DDQ under aerobic conditions.[44] Phenol was not further oxidized although electron transfer from phenol to ^{3}DDQ* occurred with the diffusion-limited rate constant. Back electron transfer from DDQ$^{•-}$ to benzene radical cation may be quite exergonic, when this process is in the Marcus inverted region,[24,45,46] where the back electron transfer is slowed down as compared to the case of phenol radical cation, which decayed by fast back electron transfer prior to the reaction with H$_2$O. Thus, the back electron transfer controls the selectivity of the reactions *via* photoinduced electron transfer.


$$(14)$$
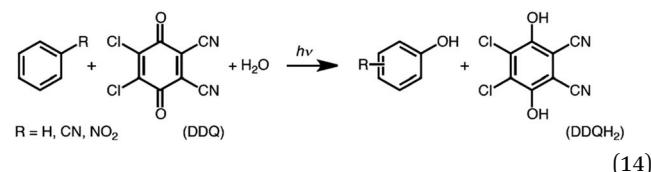
Since the singlet–triplet energy gap of Cl$_4$Q is 0.64 eV, the singlet excited state of DDQ (^{1}DDQ*) is estimated to have much stronger oxidizing ability than the triplet excited state of DDQ (^{3}DDQ*).[47] Thus, electron transfer from benzonitrile (PhCN) to ^{1}DDQ* occurs to produce DDQ$^{•-}$ and PhCN$^{•+}$ that is in equilibrium with the dimer radical cation [(PhCN)$_2$$^{•+}$] (Scheme 8).[47] The reaction of PhCN$^{•+}$ and H$_2$O occurs to form the OH-adduct radical, which is oxidized by DDQH$^•$ to produce CN-substituted phenols and DDQH$_2$ (Scheme 8).[47] The ratio of *ortho*-, *meta*- and *para*-CN-phenols produced in the photohydroxylation of benzonitrile by ^{1}DDQ*, was 44 : 18 : 38, respectively.[47] Similarly, the photohydroxylation of nitrobenzene (PhNO$_2$) also occurred *via* electron transfer from nitrobenzene to ^{1}DDQ*.[47] The ratio of *ortho*-, *meta*- and *para*-NO$_2$-phenols produced in the photohydroxylation of nitrobenzene by ^{1}DDQ*, was 45 : 40 : 15, respectively.[47]

The ratios of regioisomers were found to be determined by the electronic charges of radical cation of substrates, supported by the density functional theory.[47] For benzonitrile radical


Scheme 7 A mechanism for photohydroxylation of benzene by dioxygen with DDQ used as a photoredox catalyst in the presence of TBN and H$_2$O in MeCN under photoirradiation. Reprinted from ref. 44 with permission form American Chemical Society (Copyright 2013).

Scheme 8 Proposed mechanism for photohydroxylation of benzonitrile with DDQ and H$_2$O in MeCN *via* ^{1}DDQ*. Reprinted from ref. 47 with permission form John Wiley and Sons (Copyright 2015).

Scheme 9 Proposed mechanisms for photocatalytic C–H amination of different arenes with DDQ in the presence of TBN under photo-irradiation. Reprinted from ref. 48 with permission form John Wiley and Sons (Copyright 2017).

Scheme 10 Electrochemical generation of TAC$^{\cdot 2+}$ and photoinduced electron transfer oxidation of substrate by TAC$^{\cdot 2+}$*. Reprinted from ref. 49 with permission form the American Association for the Advancement of Science (Copyright 2021).

cation, the negative charge at the *ortho*-position is smaller than that at the *meta*-position, while the *para*-position has a positive charge.[47] As a result, OH$^-$ was mainly added to the two *ortho*-positions and a one *para*-position of benzonitrile radical cation, resulting in *ortho*- and *para*-CN-phenols, respectively.[47] However, for nitrobenzene radical cation, since the *para*-position has the largest negative charge, *other*- and *meta*-NO$_2$-phenols were mainly obtained as products in the photo-hydroxylation of nitrobenzene.[47]

DDQ has also been used as an effective photoredox catalyst with ^{t}butyl nitrite (TBN) for C–H amination of arenes by amines under visible light irradiation.[48] Two photocatalytic mechanisms are shown in Scheme 9. Electron transfer from benzene to ^{3}DDQ* occurs to produce benzene radical cation and DDQ$^{\cdot -}$ as the case of photohydroxylation of benzene (mechanism-A in Scheme 9).[48] Benzene radical cation undergoes nucleophilic attack by the amine, followed by oxidation of the resulting species by DDQH$^\cdot$ to yield the arene C–N substitution product.[48] DDQ is regenerated by TBN.[48] The radical cations generated from benzene and Cl-benzene react with various amine nucleophiles, whereas the radical cation of anisole is less reactive, yielding products with only strong nucleophiles such as pyrazole and other azoles.[48]

Alternatively the charge-transfer complex formed between amines and DDQ in the ground state may be involved (mechanism-B in Scheme 9).[48] Excitation by visible light results in hydrogen atom transfer from amines to DDQ *via* electron transfer followed by proton transfer.[48] The generated amine radical attacks the arene and another H-atom abstraction yields the product and DDQH$_2$.[48] However, the photoexcitation of the charge-transfer band at 600 nm resulted in much less product as compared with the photoexcitation of DDQ.[48] Thus, the proposed mechanism-A is more likely to be correct.

3.2. Excited states of radical dications

The higher one-electron reduction potential value than the triplet excited state of DDQ (^{3}DDQ* : E_{red}^* *vs.* SCE = 3.18 V) was reported for the excited state of a trisaminocyclopropenium radical dication (TAC$^{\cdot 2+}$: E_{red}^* *vs.* SCE = 3.33 V).[49,50] TAC$^+$ was electrochemically oxidized to form TAC$^{\cdot 2+}$, which was photo-excited with use of visible light to produce TAC$^{\cdot 2+}$* that is an excited-state species with sufficiently strong oxidizing power (3.33 V *vs.* SCE) to oxidize various substrates, including benzene and halogenated benzenes, *via* electron transfer, resulting in C–H/N–H coupling with azoles (Scheme 10).[49,50] TAC$^{\cdot 2+}$* can also convert aryl olefins to the corresponding glycol monoesters with high chemo- and diastereoselectivity.[51]

3.3. Excited states of Flavin-Sc^{3+} complexes

Metal (M^{n+}) ions acting as Lewis acids can bind to riboflavin-2′,3′,4′,5′-tetraacetate (Fl) to form the 1 : 1 and 1 : 2 complexes with Fl to metal ratios.[52] The formation constants K_1 and K_2 of the 1 : 1 and 1 : 2 complexes of Fl with Sc^{3+} were determined to be 3.1×10^4 M^{-1} and 1.4×10^3 M^{-1}, respectively.[53] The fluorescence of ^{1}(Fl-2Sc^{3+})* is quenched by electron transfer from electron donors to ^{1}(Fl-2Sc^{3+})*.[53] The quenching rate constants (k_q) of electron transfer from electron donors to ^{1}(Fl-2Sc^{3+})* increase as the 1 e$^-$ oxidation potentials (E_{ox}^0) of electron donors decrease, approaching a diffusion limited rate constant (Fig. 3).[53] The E_{red}^* (*vs.* SCE) values of Fl-M^{n+} complexes were in order of ^{1}(Fl-2Sc^{3+})* (2.45 V) > ^{1}(Fl-Yb^{3+})* (2.25 V) > ^{1}(Fl-Mg^{2+})* (2.06 V) > ^{1}Fl* (1.67 V), indicating that the order of E_{red}^* (*vs.* SCE) values of Fl-M^{n+} complexes is in agreement of the order of the Lewis acidity of M^{n+} bound to Fl.[54] The E_{red}^* value of ^{1}(Fl-2Sc^{3+})* is by 0.78 V more positive than that of ^{1}Fl* (1.67 V) due to the strong binding of two Sc^{3+} ions to Fl$^{\cdot -}$.[53] Thus, ^{1}(Fl-2Sc^{3+})* acts as a much stronger oxidant than ^{1}Fl* as shown in Fig. 3.[53] The

Fig. 3 Plots of log k_q of electron transfer from electron donors [(1) PhCH$_3$, (2) PhCH$_2$CH$_3$, (3) m-xylene, (4) o-xylene, (5) p-cymene, (6) p-xylene, (7) 1,2,3-tri-Me-benzene, (8) 1,2,4-tri-Me-benzene, (9) 1,2,3,4-tetra-Me-benzene, (10) 1,2,3,5-tetra-Me-benzene, (11) penta-Me-benzene and (12) m-di-MeO-benzene] to ^{1}Fl* (10 µM) in the absence (●) and presence of M^{n+} (1.0 × 10^{-2} M) [M^{n+} = Sc^{3+} (▲), Yb^{3+} (■) and Mg^{2+} (○)] against 1 e$^-$ oxidation potentials (E_{ox}^0) of electron donors in MeCN at 298 K. Reprinted from ref. 53 with permission form American Chemical Society (Copyright 2001).

combination of Fl with Sm^{3+} and iron complexes has also been reported to enable the visible-light driven aerobic C–H bond oxidation of alkyl benzenes.[55,56]

3.4. Excited states of Mn^{IV}(O)-(Sc^{3+})$_n$ complexes

As in the case of Fl-2Sc^{3+}, two Sc^{3+} ions are bound to the oxo moiety of a Mn^{IV}-oxo complex bearing N-benzyl-N,N',N'-tris(2-pyridylmethyl)-1,2-diamino-ethane (BnTPEN) ligand to form [(BnTPEN)Mn^{IV}(O)]$^{2+}$-(Sc(OTf)$_3$)$_2$.[57,58] Two HOTf molecules are also bound to a Mn^{IV}-oxo complex bearing N4Py ligand to form [(N4Py)Mn^{IV}(O)]$^{2+}$-(HOTf)$_2$.[59] Upon Photoexcitation of [(BnTPEN)Mn^{IV}(O)]$^{2+}$-(Sc(OTf)$_3$)$_2$ in MeCN at 298 K, the long-lived photoexcited state with the lifetime of 6.4 µs was formed.[60] When Sc(OTf)$_3$ was replaced by Sc(NO$_3$)$_3$, the lifetime of the photoexcited state of [(BnTPEN)Mn^{IV}(O)]$^{2+}$-Sc(NO$_3$)$_3$ increased to 7.1 µs.[61] Such a long-lived excited state is assigned as the doublet ^2E photoexcited state, which was formed by intersystem crossing from the ^4E excited state, due to the spin forbidden decay to the quartet ground state as reported for Mn(IV) complexes.[62,63]

The transient absorption due to ^2E excited state of [(BnTPEN) Mn^{IV}(O)]$^{2+}$-(Sc(OTf)$_3$)$_2$ decayed via electron transfer from various electron donors to the ^2E excited state to determine the rate constants of electron transfer (k_{et}).[60] Logarithm of k_{et} increases with decreasing E_{ox} values of electron donors to approach a diffusion-limited rate constant, as expressed by the Marcus equation of intermolecular electron transfer [eqn (15)],[24,25]

$$(k_{et})^{-1} = (k_{dif})^{-1} + \{Z\exp[(-\lambda/4)(1 + \Delta G_{et}/\lambda)^2/(k_B T)]\}^{-1} \quad (15)$$

where k_{dif} is the diffusion rate constant, Z is the collision frequency (10^{11} M^{-1} s^{-1}), T is the absolute temperature, k_B is the Boltzmann constant and λ is the reorganization energy of electron transfer.[60] The Gibbs energy change of electron transfer (ΔG_{et}) is given by eqn (16),

$$\Delta G_{et} = e(E_{ox} - E_{red}^*) \quad (16)$$

where E_{red}^* is the 1 e$^-$ reduction potential of the excited ^2E state of Mn^{IV}-oxo intermediate and e is the elementary charge.[60] The best fit line using eqn (15) in Fig. 4 afforded that E_{red}^* and the reorganization energy (λ) values of {[(BnTPEN)Mn^{IV}(O)]$^{2+}$-(Sc(OTf)$_3$)$_2$}* are 2.1(1) V and 0.64(4) eV, respectively.[60] The reorganization energy of electron transfer from electron donors to {[(BnTPEN)Mn^{IV}(O)]$^{2+}$-(Sc(OTf)$_3$)$_2$}* (0.64(4) eV) is much smaller than that from electron donors to the ground state of [(BnTPEN)Mn^{IV}(O)]$^{2+}$-(Sc(OTf)$_3$)$_2$ (2.11 eV).[58] Such a large difference in the λ values results from the small λ value for the ligand-center electron transfer from electron donors to {[(BnTPEN)Mn^{IV}(O)]$^{2+}$-(Sc(OTf)$_3$)$_2$}*, which corresponds to the LMCT state, {[(BnTPEN)Mn^{IV}(O)]$^{2+}$-(Sc(OTf)$_3$)$_2$}*.[60] In contrast, electron transfer from electron donors to the ground state of [(BnTPEN)Mn^{IV}(O)]$^{2+}$-(Sc(OTf)$_3$)$_2$ occurs in the Mn^{IV} center with the large λ value because of the significant change in the bond distance of Mn–O between the Mn^{IV} and Mn^{III} oxidation states.[58,59]

The highly positive E_{red}^* value of the ^2E excited state of [(BnTPEN)Mn^{IV}(O)]$^{2+}$-(Sc(OTf)$_3$)$_2$ and the small λ value enabled electron transfer from benzene (C$_6$H$_6$) to {[(BnTPEN)Mn^{IV}(O)]$^{2+}$-(Sc(OTf)$_3$)$_2$}* to generate C$_6$H$_6$$^{•+}$,[60] which forms (C$_6H_6$)$_2$$^{•+}$ in the presence of large excess C$_6$H$_6$.[64] C$_6$H$_6$$^{•+}$ reacts with H$_2$O to produce the OH adduct radical, which is oxidized by [(BnTPEN) Mn^{III}(O)]$^+$-(Sc(OTf)$_3$)$_2$ to generate PhOH with Mn^{II} species after removal of H$^+$ (Scheme 11A).[60] Mn^{II} species reacts rapidly with [(BnTPEN)Mn^{IV}(O)]$^{2+}$-(Sc(OTf)$_3$)$_2$ to form [Mn^{III}–O–Mn^{III}]$^{4+}$ species (Scheme 11B).[60]
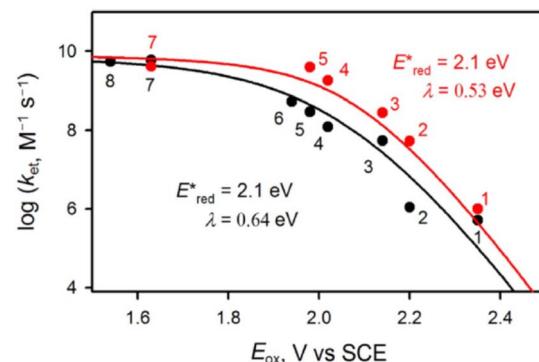
Fig. 4 Plots of log k_{et} of electron transfer from electron donors [(1) C$_6$H$_6$, (2) PhCH$_3$, (3) PhCH$_2$CH$_3$, (4) m-xylene, (5) mesitylene, (6) PhCH$_2$OH, (7) durene, and (8) naphthalene] to {[(BnTPEN)Mn^{IV}(O)]$^{2+}$-Sc(NO$_3$)$_3$}* (red circles) and {[(BnTPEN)Mn^{IV}(O)]$^{2+}$-(Sc(OTf)$_3$)$_2$}* (black circles) against E_{ox} values of electron donors in TFE/MeCN (v/v 1 : 1) at 298 K. Reprinted from ref. 61 with permission form John Wiley and Sons (Copyright 2020).
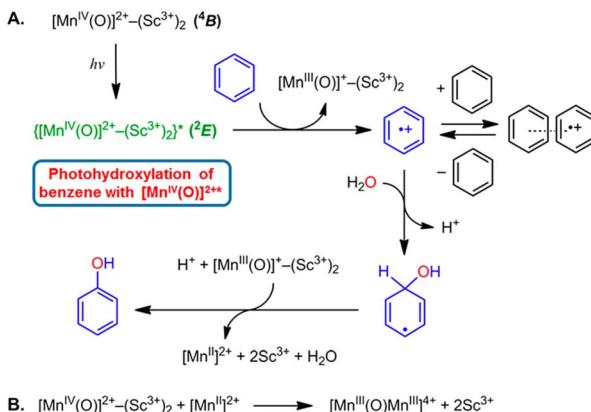
Scheme 11 (A) Proposed mechanism for the oxidation of C_6H_6 by $\{[(BnTPEN)Mn^{IV}(O)]^{2+}$-$(Sc(OTf)_3)_2\}*$.[61] (B) The formation of $[Mn^{III}$–O–$Mn^{III}]^{4+}$ species by reacting Mn^{II} with $Mn^{IV}(O)$-$(Sc^{3+})_2$. Reprinted from ref. 60 with permission form American Chemical Society (Copyright 2018).

4 PRC models

4.1. 9-Mesityl-10-methylacridinium ion

A simple electron donor–acceptor-linked molecule with a small λ value of electron transfer and a high-lying triplet excited state is an ideal PRC model compound, which has highly oxidizing and reducing capability with a long lifetime of the electron-transfer state between the electron donor and acceptor.[5] The acridinium ion (Acr^+) is the best candidate as an electron acceptor moiety in such an electron donor–acceptor-linked molecule, because the λ value of electron self-exchange between Acr^+ and its 1 e^- reduced species is the smallest (0.3 eV) among redox-active organic compounds.[5] Thus, a mesityl group (Mes) is directly linked as an electron-donor moiety at the 9-position of Acr^+ to form 9-mesityl-10-methylacridinium ion (Acr^+–Mes). According to the X-ray crystal structure of Acr^+–Mes, the mesityl moiety is orthogonal to the acridinium moiety.[65] In such a case, there is little orbital interaction between the Mes and Acr^+ moieties. Photoexcitation of Acr^+–Mes results in fast intramolecular electron transfer from the Mes moiety to the singlet excited state of the Acr^+ moiety to produce the triplet electron-transfer (ET) state ($Acr^•$–$Mes^{•+}$) via intersystem crossing.[65,66] Because the intramolecular back ET from $Acr^•$ unit to $Mes^{•+}$ unit is too slow to compete with intermolecular back ET, which obeyed second-order kinetics.[65,66] In order to obtain the lifetime due to intramolecular back ET without contribution of the intermolecular back ET, Acr^+–Mes was immobilized into tube-shaped nanosized mesoporous silica-alumina to prepare (Acr^+–Mes@tAlMCM-41) by cation exchange.[67] Photoirradiation of Acr^+–Mes@tAlMCM-41 ($\lambda > 390$ nm) at 298 K results in formation of the triplet ET state $[^3(Acr^•$–$Mes^{•+})*]$ via photoinduced ET from the Mes moiety to $^1(Acr^+)*$ moiety (Fig. 5A).[67] The EPR spectrum of $^3(Acr^•$–$Mes^{•+})*$@tAlMCM-41 was confirmed by overlapping the EPR signals of the $Acr^•$ and $Mes^{•+}$ moieties (Fig. 5B and C, respectively).[67] The decay in the EPR signal intensity due to $^3(Acr^•$–$Mes^{•+})*$ followed first-order kinetics (Fig. 5D) to give the lifetime of 3 s for the intramolecular back
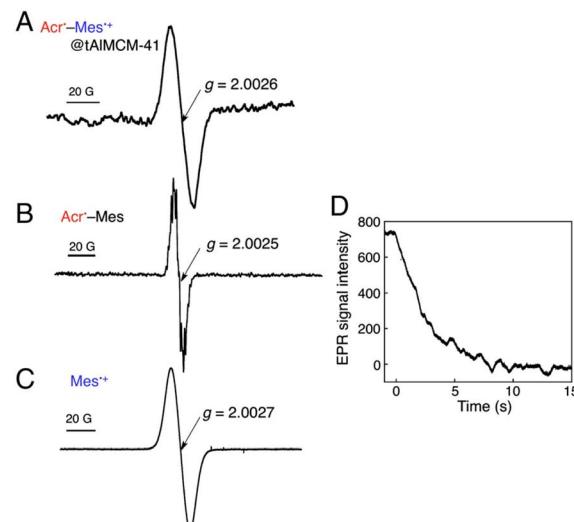
**Fig. 5** (A) EPR spectrum of $Acr^•$–$Mes^{•+}$@tAlMCM-41 in MeCN at 298 K observed under photoirradiation ($\lambda > 390$ nm) for 2 min. (B) EPR spectrum of $Acr^•$–Mes generated by the photoinduced ET reduction of Acr^+–Mes by BNAH (5.0 equiv.) in MeCN under photoirradiation. (C) EPR spectrum of mesitylene radial cation prepared by the photoinduced 1 e^- oxidation of mesitylene with $Hg(CF_3COO)_2$ in CF_3COOH at 298 K under photoirradiation. (D) Decay time course of the EPR signal intensity due to $Acr^•$–$Mes^{•+}$@tAlMCM-41 in MeCN at 298 K. Reprinted with permission from ref. 67. Copyright 2012, National Academy of Sciences.

ET in deaerated MeCN at 298 K.[67] The lifetime of 3 s is the longest reported so far and is longer than the charge-separated state lifetime in the PRCs.[67]

4.2. PS-II model

The first functional model of PS-II was reported for the photocatalytic reduction of p-benzoquinone derivatives [X–Q: DDQ, p-benzoquinone (Q), Cl_4Q, 2,5-di-Me-p-benzoquinone (PXQ) and duroquinone (DQ)] as plastoquinone analogs with the concomitant $4e^-/4H^+$ oxidation of water to evolve O_2 [eqn (17)] in the presence of $[Fe^{II}(N4Py)]^{2+}$ (N4Py = 1,1-di(pyridin-2-yl)-N,N-bis(pyridin-2-ylmethyl)methanamine)[68] acting as a water oxidation catalyst (WOC).[69]

$$2H_2O + 2DDQ \xrightarrow[[(N4Py)Fe^{II}]^{2+}]{h\nu} O_2 + 2DDQH_2 \quad (17)$$
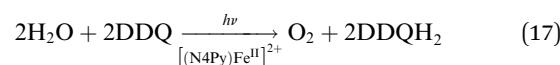
The photocatalytic mechanism of the oxidation of H_2O by DDQ with $[(N4Py)Fe^{II}]^{2+}$ is shown in Scheme 12.[69] Electron transfer from iron(II) complex to $^3DDQ*$ with H_2O occurs to form $Fe^{III}(OH)$ and $DDQH^•$ species (Scheme 12, pathway a). Subsequent electron transfer from $Fe^{III}(OH)$ to $^3DDQ*$ occurs to form $Fe^{IV}(O)$ and $DDQH^•$ species (Scheme 12, pathway b).[70–72] Finally electron transfer from $Fe^{IV}(O)$ to $^3DDQ*$ also occurs to generate $Fe^V(O)$ intermediate (Scheme 12, pathway c).[69] From the slope of plot of the decay rate constant of $^3DDQ*$ against concentration of iron(IV)-oxo, the second-order rate constant of electron transfer from iron(IV)-oxo to $^3DDQ*$ was determined to
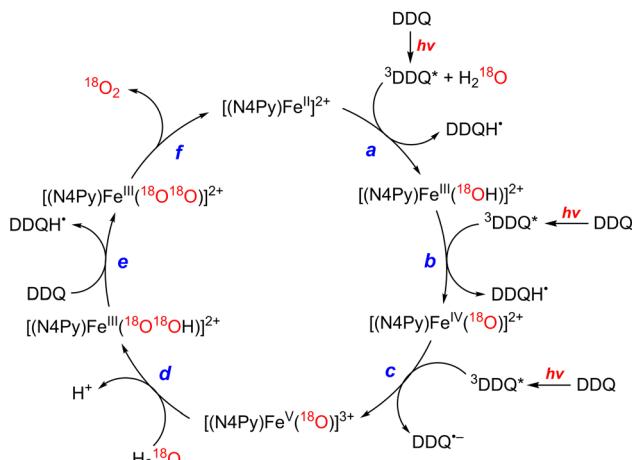
Scheme 12 A mechanism of the photocatalytic $4e^-/4H^+$ oxidation of H_2O by DDQ as an oxidant and $[Fe^{II}(N4Py)]^{2+}$ as a WOC. Reprinted from ref. 69 with permission form American Chemical Society (Copyright 2019).

Scheme 13 (a) Plastoquinol and its analogs.[84] (b) Photocatalytic hydrogen evolution using the PS-I model system consisting of hydroquinone derivatives, 9-mesityl-10-methylacridinium ion as a PRC model and $Co^{III}(dmgH)_2pyCl$. Reprinted from ref. 87 with permission form American Chemical Society (Copyright 2020).

be 9.4×10^9 M^{-1} s^{-1}.[69] Iron(v)-oxo reacts rapidly with H_2O to produce $Fe^{III}(OOH)$ species and H^+ (Scheme 12, pathway d).[69] On the other hand, DDQH$^{\bullet}$ disproportionates to produce DDQ and DDQH$_2$.[69] $Fe^{III}(OOH)$ is oxidized thermally by DDQ via H-atom transfer to produce iron(iii)-superoxo species, $Fe^{III}(O_2^{\bullet-})$ (Scheme 12, pathway e), accompanied by release of O_2 and regeneration of iron(ii) complex (Scheme 12, pathway f).[69] Meanwhile $[(N4Py)Fe^{III}(OOH)]^{2+}$ can be generated independently from the reaction of $[(N4Py)Fe^{II}]^{2+}$ and H_2O_2,[72] and the production of O_2 was confirmed through a thermal reaction between $[(N4Py)Fe^{III}(OOH)]^{2+}$ and DDQ, indicating that $[(N4Py)Fe^{III}(OOH)]^{2+}$ is thermally oxidized by DDQ.[69]

The rate constants of electron transfer from $[(N4Py)Fe^{IV}(O)]^{2+}$ to other $^3X–Q^*$ derivatives were also determined to be close to the diffusion limited value.[69] Thus, X–Q can oxidize H_2O to O_2 with Fe(ii) complex under photoirradiation in the PS-II model reactions.[69]

4.3. PS-I model

Because of the extremely long lifetime of Acr$^{\bullet}$–Mes$^{\bullet+}$ with the strong oxidizing and reducing capability, Acr$^+$–Mes has acted an efficient organic photoredox catalyst in various organic transformations, which have been reviewed well.[73–82] One notable example is the combination of a PRC model (Acr$^+$–Mes) and an H_2 evolution catalyst $[Co^{III}(dmgH)_2pyCl$ (py = pyridine and dmgH$^-$ = N,N'-Dihydroxy-2,3-butanediimine monoanion)],[83–86] which mimics the photocatalytic function of PS-I (Scheme 13).[87] Solar energy is harvested by the Acr$^+$ moiety of Acr$^+$–Mes to generate ^{3}(Acr$^{\bullet}$–Mes$^{\bullet+}$).[87] Electron transfer from QH_2 to the Mes$^{\bullet+}$ unit of ^{3}(Acr$^{\bullet}$–Mes$^{\bullet+}$) occurs with the diffusion-limited value to form Acr$^{\bullet}$–Mes and X–QH$_2^{\bullet+}$. Then, electron transfer from Acr$^{\bullet}$–Mes to Co^{III} complex (i.e., $Co^{III}(dmgH)_2pyCl$) occurs to generate Co^{II} species, accompanied by reproduction of Acr$^+$–Mes.[87] $QH_2^{\bullet+}$ is deprotonated rapidly to produce semiquinone radical (QH$^{\bullet}$).[87] Then proton-coupled electron transfer (PCET) from QH$^{\bullet}$ to Co^{II} species occurs to form Q and the Co^{III}–H$^-$
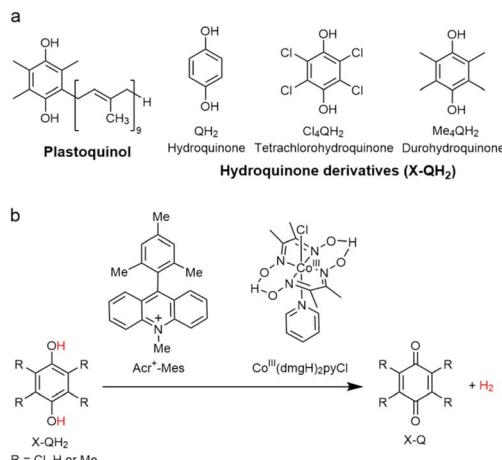
species that reacts with H^+ to evolve H_2, accompanied by reproduction of an H_2 evolution catalyst ($Co^{III}(dmgH)_2pyCl$).[87] The deuterium kinetic isotope effect (KIE = 2.0) was observed for the H_2 evolution rate by use of D_2O instead of H_2O.[88,89] This indicates that PCET from QH$^{\bullet}$ (QD$^{\bullet}$) to Co^{II} species may be the rate-determining step for the photocatalytic H_2 evolution in the PS-I model reaction.[87]

4.4. Combination of PS-I and PS-II molecular models

A PS-II molecular model (Scheme 12) has been combined with a PS-I molecular model (Scheme 14) to mimic the photocatalytic function of photosynthesis as shown in Fig. 6a, where the two cells for PS-I and PS-II molecular models were connected in a H_2O-TFE phase with use of a glass membrane.[90] Only hydroquinone (QH_2) derivatives can pass through the glass membrane, but other catalysts cannot.[90] Photoirradiation of a H_2O–TFE/toluene solution containing $[(N4Py)Fe^{II}]^{2+}$ and quinone in the left cell as well as a H_2O–TFE/toluene solution containing Acr$^+$–Mes and $Co^{III}(dmgH)_2pyCl$ in the right cell (Fig. 6a) resulted in evolution of O_2 and H_2 from the left and right cells, respectively (Fig. 6b and c), with 100% yield in both cases on the basis of the initial concentration of quinone (Q) in accordance with the stoichiometry of mimicry of photosynthesis [eqn (18)].[90]

$$2H_2O \xrightarrow[\text{Acr}^+-\text{Mes}/Co^{III}(dmgH)_2pyCl]{h\nu/Q/[(N4Py)Fe^{II}]^{2+}} O_2 + 2H_2 \quad (18)$$
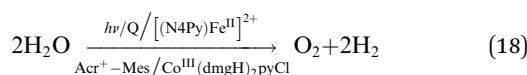
When the toluene phases of the left and right cells are connected with a glass filter (Fig. 7a), photoirradiation of both parts resulted in formation of much larger amounts of H_2 (Fig. 7b) as compared with the initial concentration of quinone.[90] The turnover number for the H_2 evolution were 160 ± 21 on the basis of the initial concentration of quinone.[90] Thus, quinone
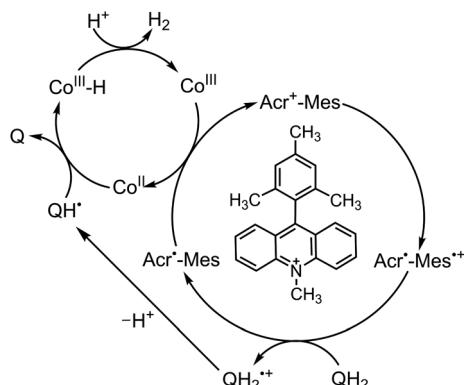
Scheme 14 Proposed PS-I model mechanism of photocatalytic H_2 evolution from hydroquinone (QH_2) derivatives with Acr^+–Mes and Co^{III} complex. Reprinted from ref. 87 with permission form American Chemical Society (Copyright 2020).
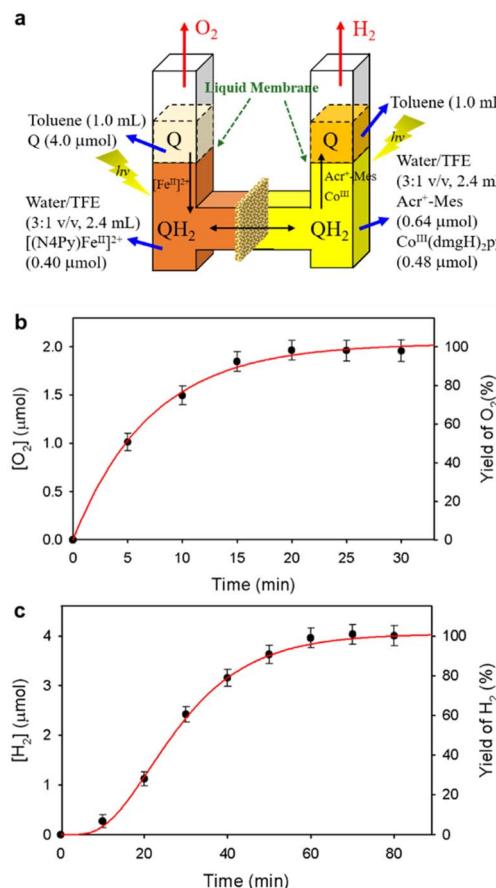

Fig. 6 (a) A photocatalytic system used an H-type cell for the photocatalytic production of H_2 and O_2 from H_2O. (b) Time profile of the production of O_2 in the photocatalytic H_2O oxidation. (c) Time profile of the production of H_2 in the photocatalytic H_2O reduction. Reprinted from ref. 90 with permission form American Chemical Society (Copyright 2022).

acts as a photocatalyst for photocatalytic H_2O splitting as shown in Scheme 15.[90] This is the first case to achieve photocatalytic H_2O splitting to produce H_2 and O_2 by combining the molecular
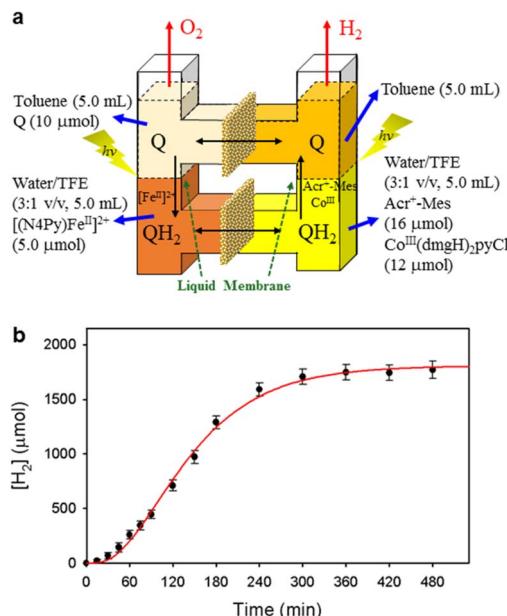
Fig. 7 (a) A photochemical cell used for photocatalytic production of H_2 and O_2 from H_2O. (b) Time profile of the production of H_2 in the photocatalytic H_2O splitting under photoirradiation. Reprinted from ref. 90 with permission form American Chemical Society (Copyright 2022).
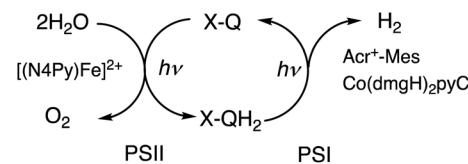
Scheme 15 A scheme for the photocatalytic production of H_2 and O_2 from H_2O by the combination of the molecular models of PS-I and PS-II with use of X–Q/X–QH_2 as plastoquinone/plastoquinol analogue in photosynthesis. Reprinted from ref. 90 with permission form American Chemical Society (Copyright 2022).

models of PS-I and PS-II in homogeneous catalytic system (*e.g.*, in solution).

5 Conclusions

The excited states of organic electron donors become much stronger electron donors as compared with the ground states, undergoing various reduction reactions, which would otherwise be impossible to occur at the ground states. For example, the singlet excited state of an NADH (dihydronicotinamide adenine dinucleotide) analog, 9,10-dihydro-10-methylacridine ($^1AcrH_2^*$) has a largely negative one-electron reduction potential (E_{red}^* *vs.* SCE = –3.1 V) and a lifetime of 7.0 ns to enable to reduce various alkyl halides. The more negative E_{red}^* value (−3.36 V) is evaluated for the doublet excited state of stable acridinyl radical (Mes–Acr$^\bullet$), which acts as a super-reductant. The excited states of radical anions and anions also act as super-reductants that enabled to reduce substrates, which are

usually difficult to be reduced by the ground state reductants. By the same token, the excited states of organic electron acceptors such as DDQ and TAC$^{\cdot 2+}$ become much stronger electron acceptors as compared with the ground states, undergoing various oxidation reactions, which would otherwise be impossible to occur at the ground states. The binding of Sc^{3+} ions to flavin and $Mn(IV)$-oxo complexes enhanced the oxidizing ability. The excited state further enhanced the oxidizing ability, acting as super-oxidants.

A simple electron donor–acceptor-linked molecule with a small reorganization energy of electron transfer such as Acr^+–Mes acts as an ideal photosynthetic reaction center (PRC) model compound, which has high oxidizing and reducing capability with a long lifetime of the ET state. The PCR model compound was used to construct a PS-I model system in which H_2 was evolved from plastoquinol analogues with a cobalt complex as an H_2 evolution catalyst.

The PS-I model was combined with a PS-II model with use of the excited state of plastoquinone analogues and water oxidation catalyst to achieve the photofunction of photosynthesis. Because H_2 can reduce NAD^+ to NADH by redox catalysis of metal complexes,[91,92] NADH can be produced from water by adding to NAD^+ reduction catalysts to the molecular photocatalytic system in Scheme 15. By the same token, CO_2 can be reduced by water by adding CO_2 reduction catalysts[93–95] to the molecular photocatalytic system in Scheme 15. Thus, redox catalysis *via* photoinduced electron transfer discussed in this perspective may further be expanded to construct more useful photocatalytic systems for solar fuel production and green redox reactions. The development of stronger super reductants and super oxidants together with PRC models with the stronger reducing and oxidizing power would further expand the scope of redox catalysis *via* photoinduced electron transfer.

Author contributions

All the authors contributed to the discussion, editing and revision of this work.

Conflicts of interest

There are no conflicts to declare.

Acknowledgements

Notes and references

1 R. Croce and H. van Amerongen, *Science*, 2020, **369**, eaay2058.

2 J.-R. Shen, *Annu. Rev. Plant Biol.*, 2015, **66**, 23–48.

3 M. M. Najafpour, I. Zaharieva, Z. Zand, S. M. Hosseini, M. Kouzmanova, M. Hołyńska, I. Tranca, A. W. Larkum, J.-R. Shen and S. I. Allakhverdiev, *Coord. Chem. Rev.*, 2020, **409**, 213183.

4 M. M. Najafpour and S. I. Allakhverdiev, *J. Photochem. Photobiol., B*, 2015, **152**, 173–424.

5 S. Fukuzumi, K. Ohkubo and T. Suenobu, *Acc. Chem. Res.*, 2014, **47**, 1455–1464.

6 S. Fukuzumi, *Org. Biomol. Chem.*, 2003, **1**, 609–620.

7 M. J. Llansola-Portoles, D. Gust, T. A. Moore and A. L. Moore, *C. R. Chim.*, 2017, **20**, 296–313.

8 S. Fukuzumi and K. Ohkubo, *J. Mater. Chem.*, 2012, **2**, 4575–4587.

9 O. Ito and F. D'Souza, *Molecules*, 2012, **17**, 5816–5835.

10 S. Fukuzumi, *Phys. Chem. Chem. Phys.*, 2008, **10**, 2283–2297.

11 D. Gust, T. A. Moore and A. L. Moore, *Acc. Chem. Res.*, 2009, **42**, 1890–1898.

12 S. Fukuzumi and T. Kojima, *J. Mater. Chem.*, 2008, **18**, 1427–1439.

13 C. B. KC and F. D'Souza, *Coord. Chem. Rev.*, 2016, **322**, 104–141.

14 M. E. El-Khouly, E. El-Mohsnawy and S. Fukuzumi, *J. Photochem. Photobiol. C.: Photochem. Rev.*, 2017, **31**, 36–83.

15 S. Fukuzumi, Y.-M. Lee and W. Nam, *Biochem. Soc. Trans.*, 2018, **46**, 1279–1288.

16 A. Zieleniewska, F. Lodermeyer, A. Roth and D. M. Guldi, *Chem. Soc. Rev.*, 2018, **47**, 702–714.

17 S. Fukuzumi, Y.-M. Lee and W. Nam, *Tetrahedron*, 2020, **76**, 131024.

18 C. K. Prier, D. A. Rankic and D. W. C. MacMillan, *Chem. Rev.*, 2013, **113**, 5322–5363.

19 N. Corrigan, S. Shanmugam, J. Xu and C. Boyer, *Chem. Soc. Rev.*, 2016, **45**, 6165–6212.

20 A. Soupart, F. Alary, J.-L. Heully, P. I. P. Elliott and I. M. Dixon, *Coord. Chem. Rev.*, 2020, **408**, 213184.

21 S. Fukuzumi, *Electron Transfer: Mechanisms and Applications*, Wiley-VCH, Weinheim, 2020.

22 S. Fukuzumi and K. Ohkubo, *Org. Biomol. Chem.*, 2014, **12**, 6059–6071.

23 S. Fukuzumi and K. Ohkubo, *Chem. Sci.*, 2013, **4**, 561–574.

24 R. A. Marcus, *Annu. Rev. Phys. Chem.*, 1964, **15**, 155–196.

25 R. A. Marcus, *Angew. Chem., Int. Ed. Engl.*, 1993, **32**, 1111–1121.

26 R. A. Marcus and N. Sutin, *Biochim. Biophys. Acta*, 1985, **811**, 265–322.

27 N. Ishikawa and S. Fukuzumi, *J. Am. Chem. Soc.*, 1990, **112**, 8864–8870.

28 C. P. Andrieux, C. Blocman, J. M. Dumas-Bouchiat, F. M'Halla and J. M. Savéant, *J. Am. Chem. Soc.*, 1980, **102**, 3806–3813.

29 B. Huang, X.-S. Bu, J. Xu, J.-J. Dai, Y.-S. Feng and H.-J. Xu, *Asian J. Org. Chem.*, 2018, **7**, 137–140.

30 J. Jiang, W.-M. Zhang, J.-J. Dai, J. Xu and H.-J. Xu, *J. Org. Chem.*, 2017, **82**, 3622–3630.

31 S. Fukuzumi, K. Hironaka and T. Tanaka, *J. Am. Chem. Soc.*, 1983, **105**, 4722–4727.

32 Q. Huang, J.-W. Wu and H.-J. Xu, *Tetrahedron Lett.*, 2013, **54**, 3877–3881.

33 H.-J. Xu, Y.-C. Liu, Y. Fu and Y.-D. Wu, *Org. Lett.*, 2006, **8**, 3449–3451.

34 S. Fukuzumi, S. Koumitsu, K. Hironaka and T. Tanaka, *J. Am. Chem. Soc.*, 1987, **109**, 305–316.

35 S. Fukuzumi, Y. Tokuda, T. Kitano, T. Okamoto and J. Otera, *J. Am. Chem. Soc.*, 1993, **115**, 8960–8968.

36 S. Fukuzumi, K. Ohkubo, T. Suenobu, K. Kato, M. Fujitsuka and O. Ito, *J. Am. Chem. Soc.*, 2001, **123**, 8459–8467.

37 I. A. MacKenzie, L. Wang, N. P. R. Onuska, O. F. Williams, K. Begam, A. M. Moran, B. D. Dunietz and D. A. Nicewicz, *Nature*, 2020, **586**, 76–80.

38 I. Ghosh, T. Ghosh, J. I. Bardagi and B. König, *Science*, 2014, **346**, 725–728.

39 C. J. Zeman, S. Kim, F. Zhang and K. S. Schanze, *J. Am. Chem. Soc.*, 2020, **142**, 2204–2207.

40 S. Farid, J. P. Dinnocenzo, P. B. Merkel, R. H. Young, D. Shukla and G. Guirado, *J. Am. Chem. Soc.*, 2011, **133**, 11580–11587.

41 D. Rehm and A. Weller, *Isr. J. Chem.*, 1970, **8**, 259–271.

42 H. Kim, H. Kim, T. H. Lambert and S. Lin, *J. Am. Chem. Soc.*, 2010, **142**, 2087–2092.

43 A. J. Rieth, M. I. Gonzalez, B. Kudisch, M. Nava and D. G. Nocera, *J. Am. Chem. Soc.*, 2021, **143**, 14352–14359.

44 K. Ohkubo, A. Fujimoto and S. Fukuzumi, *J. Am. Chem. Soc.*, 2013, **135**, 5368–5371.

45 S. Fukuzumi, K. Ohkubo, H. Imahori and D. M. Guldi, *Chem. – Eur. J.*, 2003, **9**, 1585–1593.

46 M. Murakami, K. Ohkubo and S. Fukuzumi, *Chem. – Eur. J.*, 2010, **16**, 7820–7832.

47 K. Ohkubo, K. Hirose and S. Fukuzumi, *Chem. – Eur. J.*, 2015, **21**, 2855–2861.

48 S. Das, P. Natarajan and B. König, *Chem. – Eur. J.*, 2017, **23**, 18161–18165.

49 T. Shen and T. H. Lambert, *Science*, 2021, **371**, 620–626.

50 H. Huang, Z. M. Strater, M. Rauch, J. Shee, T. J. Sisto, C. Nuckolls and T. H. Lambert, *Angew. Chem., Int. Ed.*, 2019, **58**, 13318–13322.

51 H. Huang and T. H. Lambert, *J. Am. Chem. Soc.*, 2021, **143**, 7247–7252.

52 S. Fukuzumi, S. Kuroda and T. Tanaka, *J. Am. Chem. Soc.*, 1985, **107**, 3020–3027.

53 S. Fukuzumi, K. Yasui, T. Suenobu, K. Ohkubo, M. Fujitsuka and O. Ito, *J. Phys. Chem. A*, 2001, **105**, 10501–10510.

54 S. Fukuzumi and K. Ohkubo, *Chem. – Eur. J.*, 2000, **6**, 4532–4535.

55 M. S. S. V. Mouli, S. Katyal and A. K. Mishra, *Synlett.*, 2022, DOI: 10.1055/a-1928-3417.

56 B. Mühldorf and R. Wolf, *Angew. Chem., Int. Ed.*, 2016, **55**, 427–430.

57 J. Chen, Y.-M. Lee, K. M. Davis, X. Wu, M. S. Seo, K.-B. Cho, H. Yoon, Y. J. Park, S. Fukuzumi, Y. N. Pushkar and W. Nam, *J. Am. Chem. Soc.*, 2013, **135**, 6388–6391.

58 H. Yoon, Y.-M. Lee, X. Wu, K.-B. Cho, R. Sarangi, W. Nam and S. Fukuzumi, *J. Am. Chem. Soc.*, 2013, **135**, 9186–9194.

59 J. Chen, H. Yoon, Y.-M. Lee, M. S. Seo, R. Sarangi, S. Fukuzumi and W. Nam, *Chem. Sci.*, 2015, **6**, 3624–3632.

60 N. Sharma, J. Jung, K. Ohkubo, Y.-M. Lee, M. E. El-Khouly, W. Nam and S. Fukuzumi, *J. Am. Chem. Soc.*, 2018, **140**, 8405–8409.

61 N. Sharma, Y.-M. Lee, W. Nam and S. Fukuzumi, *Isr. J. Chem.*, 2020, **60**, 1049–1056.

62 R. W. Kitzmann, J. Moll and K. Heinze, *Photochem. Photobiol. Sci.*, 2022, **21**, 1309–1331.

63 V. Baslon, P. J. Harris, C. Reber, E. H. Colmer, A. T. Jackson, P. A. Forshaw, M. J. Smith, R. Adam Kinney and J. Teser, *Can. J. Chem.*, 2017, **95**, 547–552.

64 P. B. Merkel, P. Luo, J. P. Dinnocenzo and S. Farid, *J. Org. Chem.*, 2009, **74**, 5163–5173.

65 S. Fukuzumi, H. Kotani, K. Okubo, S. Ogo, N. V. Tkachenko and H. Lemmetyinen, *J. Am. Chem. Soc.*, 2004, **126**, 1600–1601.

66 T. Tsudaka, H. Kotani, K. Ohkubo, T. Nakagawa, N. V. Tkachenko, H. Lemmetyinen and S. Fukuzumi, *Chem. – Eur. J.*, 2017, **23**, 1306–1317.

67 S. Fukuzumi, K. Doi, A. Itoh, T. Suenobu, K. Ohkubo, Y. Yamada and K. D. Karlin, *Proc. Natl. Acad. Sci. U.S.A.*, 2012, **109**, 15572–15577.

68 J. Kaizer, E. J. Klinker, N. Y. Oh, J.-U. Rohde, W. J. Song, A. Stubna, J. Kin, E. Münck, W. Nam and L. Que Jr., *J. Am. Chem. Soc.*, 2004, **126**, 472–473.

69 Y. H. Hong, J. Jung, T. Nakagawa, N. Sharma, Y.-M. Lee, W. Nam and S. Fukuzumi, *J. Am. Chem. Soc.*, 2019, **141**, 6748–6754.

70 H. Kotani, T. Suenobu, Y.-M. Lee, W. Nam and S. Fukuzumi, *J. Am. Chem. Soc.*, 2011, **133**, 3249–3251.

71 S. Fukuzumi, T. Kojima, Y.-M. Lee and W. Nam, *Coord. Chem. Rev.*, 2017, **333**, 44–56.

72 S. Hong, Y.-M. Lee, W. Shin, S. Fukuzumi and W. Nam, *J. Am. Chem. Soc.*, 2009, **131**, 13910–13911.

73 D. A. Nicewicz and T. M. Nguyen, *ACS Catal.*, 2014, **4**, 355–360.

74 N. A. Romero and D. A. Nicewicz, *Chem. Rev.*, 2016, **116**, 10075–10166.

75 K. A. Margrey and D. A. Nicewicz, *Acc. Chem. Res.*, 2016, **49**, 1997–2006.

76 N. A. Romero, K. A. Margrey, N. E. Tay and D. A. Nicewicz, *Science*, 2015, **349**, 1326–1330.

77 N. Holmberg-Douglas and D. A. Nicewicz, *Chem. Rev.*, 2022, **122**, 1925–2016.

78 X. Zhang, K. P. Pakesh, L. Ravindar and H.-L. Quin, *Green Chem.*, 2018, **20**, 4790–4833.

79 A. Vega-Peñaloza, J. Mateos, X. Companyó, M. Escudero-Casao and L. Dell'Amico, *Angew. Chem., Int. Ed.*, 2021, **60**, 1082–1097.

80 A. Tlili and S. Lakhdar, *Angew. Chem., Int. Ed.*, 2021, **60**, 2–26.

81 T. Bortolato, S. Cuadros, G. Simionato and L. Dell'Amico, *Chem. Commun.*, 2022, **58**, 1263–1283.

82 M. V. Bobo, J. J. Kuchta III and A. K. Vannucci, *Org. Biomol. Chem.*, 2021, **19**, 4816–4834.

83 J. L. Dempsey, B. S. Brunschwig, J. R. Winkler and H. B. Gray, *Acc. Chem. Res.*, 2009, **42**, 1995–2004.

84 S. Fukuzumi, Y.-M. Lee and W. Nam, *Coord. Chem. Rev.*, 2018, **355**, 54–73.

85 D. Dolui, S. Khandelwal, P. Majumder and A. Dutta, *Chem. Commun.*, 2020, **56**, 8166–8181.

86 G. Zhang, X. Hu, C.-W. Chiang, H. Yi, P. Pei, A. K. Singh and A. Lei, *J. Am. Chem. Soc.*, 2016, **138**, 12037–12040.

87 Y. H. Hong, Y.-M. Lee, W. Nam and S. Fukuzumi, *Inorg. Chem.*, 2020, **59**, 14838–14846.

88 S. Fukuzumi, Y.-M. Lee and W. Nam, *Bull. Korean Chem. Soc.*, 2021, **42**, 1558–1568.

89 S. Fukuzumi, Y.-M. Lee and W. Nam, *Bull. Korean Chem. Soc.*, 2020, **41**, 1217–1232.

90 Y. H. Hong, Y.-M. Lee, W. Nam and S. Fukuzumi, *J. Am. Chem. Soc.*, 2022, **144**, 695–700.

91 Y. Maenaka, T. Suenobu and S. Fukuzumi, *J. Am. Chem. Soc.*, 2012, **134**, 367–374.

92 S. Fukuzumi, Y.-M. Lee and W. Nam, *J. Inorg. Biochem.*, 2019, **199**, 110777.

93 S. Fukuzumi, Y.-M. Lee, H. S. Ahn and W. Nam, *Chem. Sci.*, 2018, **9**, 6017–6034.

94 L. Chen, G. Chen, C.-F. Leung, C. Cometto, M. Robert and T.-C. Lau, *Chem. Soc. Rev.*, 2020, **49**, 7271–7283.

95 T. Kojima, *ChemPhotoChem*, 2021, **5**, 512–520.